Petroleum and Coal

Article **Open Access**

Modeling Surge pressures during tripping operations in a concentric annulus

Zakarya Belimane[1], Ahmed Hadjadj[1], Hicham Ferroudji[1] and Mohammad Azizur Rahman[2]

[1] *Laboratory of Petroleum Equipment's Reliability and Materials, Hydrocarbons and Chemistry Faculty, Université M'Hamed Bougara, Boumerdès, Algeria*
[2] *Department of Petroleum Engineering, Texas A&M University at Qatar, Qatar*

Received July 16, 2021; Accepted January 14, 2022

Abstract

This paper aims to estimate surge pressure resulting from the flow of a Herschel-Bulkley fluid through concentric annuli during tripping operations. A semi-analytical model which includes new constraints to avoid non-physical solutions was developed then solved numerically . Moreover, a numerical model was implemented using finite difference method for which accurate solutions were obtained. Besides, the commercial software (Ansys-Fluent 19R3) was employed. The results are compared with existing experimental data from literature where a good agreement is observed with a maximum average relative error of 4% and 7.8% for the two studied drilling fluids, respectively. These models were successfully extended to power-law fluids. On the other hand, numerical results were collected by varying the relevant drilling parameters. The outputs indicated that the increase in the pipe tripping velocity causes an increase of the surge pressure independently of the parameter of interest, however, the rate of increase changes from one parameter to another. Based on this parametric study, a surrogate model using the Random Forest algorithm is constructed. This model predicts surge and swab pressures without requiring cumbersome numerical calculations. The model predictions have shown a satisfactory matching with an R^2 equals to 0.99 for both training and test data.

Keywords*: Surge and Swab pressures; Concentric annuli; Semi-analytical model; Numerical model; Surrogate model and Machine Learning; Yield Power Law (YPL) and Power Law (PL).*

1. Introduction

The attention towards studying wellbore hydraulics has increased recently as new technologies such as deep-water drilling have emerged in the industry since they present several challenges associated with controlling the downhole pressure caused by the narrow limits between fracture and pore pressures. Thus, the estimation of these pressures within these narrow margins plays an important role in many phases of well drilling, especially while tripping. During drilling operations, drillers may be forced to pull out the drill string for different reasons such as changing the drill bit or performing logging operations. At the end of these operations, the drill string must be returned back to the borehole. During these tripping operations, the drill string behaves like a piston that translates axially through the borehole, this translation causes pressure perturbations. High tripping-out speeds can cause a decrease (swab) in the wellbore pressure, while, high tripping-in speeds may induce an increase (surge) in the wellbore pressure. Thus, formation fracturing and loss of circulation might be provoked due to high surge pressures. Also, because of high swab pressures, fluid formation may enter the wellbore which may induce kicks. Low tripping speeds may reduce the effect of these pressures, however, this will increase the Non-Productive-Time (NPT) and therefore cost. For that, an accurate prediction of these pressures can help engineers to find a balance by estimating the maximum allowable tripping speeds to both, reduce the NPT and keep the wellbore pressure within the margin to prevent drilling problems.

In steady-state models, drilling fluids are assumed to react instantaneously with the drill pipe movement and develop fully established flows. In this case, researchers consider the

viscous dissipation term only in the momentum equation to calculate pressure losses, while transient models are more complicated and include inertial effects [1]. To calculate surge and swab pressures, momentum, mass conservation equations, and an appropriate constitutive law for non-Newtonian drilling fluid are solved using different methods such as semi-analytical, numerical methods, narrow-slot approximation, etc.

Numerous studies were conducted to study the influence of the different drilling parameters on surge and swab pressures [2-4], results show that these pressures depend on drillpipe speed, pipe and borehole diameters, fluid rheology, flow regime, and whether the pipe at the drill bit is fully open or fully closed. Other influencing factors such as borehole geometry irregularities such as eccentric and partially-blocked ones and dynamic effects play also an important role.

The surge and swab pressures have been extensively analyzed to build mathematical models under different drilling working conditions. At early stages, studies focused on explaining the causes and problems resulting from the tripping operations, then, computational models were developed to accurately predict the pressures resulting from these operations. Different methods were used to estimate these pressures such as field tests, experimental measurement, and modeling based on mathematical methods including correlations, semi-analytical, numerical, and narrow-slot approximation technique. The outcome of the developed numerical and experimental results was used to establish regression models for predicting surge pressure for the flow of different non-Newtonian drilling fluids through concentric annulus without requiring a numerical procedure [3,5-6]. However, other existing models [2,7-9] require cumbersome numerical procedures to establish their prediction models.

Early studies tried to explain the causes of the drilling issues related to surge and swab pressures. Cannon [10] and Goins Jr *et al.* [11] demonstrated that due to enormous downhole pressure perturbations caused by tripping the drill string with high velocities, drilling problems such as formation fracture caused by fluid filtration from the wellbore and kicks caused by fluid influx into the wellbore may occur. Another study of Cardwell Jr [12] presented the first quantitative technique to predict these pressures in the case of Newtonian fluids in both laminar and turbulent regimes, but they took into account the pressure losses caused by the moving fluid viscous effects through an annulus with a stationary drill pipe. Clark Jr [13] calculated pressure losses caused by the inertial effects and viscous drag for the flow of Bingham plastic fluid through a concentric annulus with moving inner pipe for both laminar and turbulent flow regimes. Burkhardt [5] used a semi-analytical method to model steady-state surge pressures caused by Bingham Plastic fluid flow through a concentric annulus with Open-Ended Pipe (OEP) and Closed-Ended Pipe (CEP) in vertical wells. Schuh [6] used a numerical model to accurately model the flow of PL fluids through an annulus with CEP. Fontenot and Clark [14] developed a model for computing surge and swab pressures for both Bingham Plastic and PL fluids in which the comparison against field data shows a satisfactory agreement.

Transient models have been developed [1,15-16] to estimate downhole pressure variations while running in and out the drill pipe. These models take into consideration the neglected dynamic effects in steady-state models such as inertial effects, fluid compressibility, and the drill pipe compressibility and elasticity. The transient models results show that steady-state models overestimate the pressure surges.

Osorio and Steffe [8] established a semi-analytical model to predict surge pressure for Herschel-Bulkley fluids in a concentric annulus with back extrusion which is a similar problem to the surge phenomenon during tripping in drilling. Haige and Xisheng [9] used Robertson-Stiff rheological model to estimate the resulting surge pressures in directional wells using a theoretical model. The solutions of this model were obtained numerically then plotted in form of curves. Moreover, He *et al.* [17] developed semi-analytical models for predicting surge and swab pressures in a concentric annulus. Then, they investigated the effect of different drilling parameters such as rheological properties, annular geometry, and pipe velocity on surge and swab pressures.

To develop a mathematical model of a drilling fluid flow through an annular space, the narrow-slot approximation technique was introduced. It can be used to predict surge and swab

pressures where the drill string and casing are represented by two parallel plates separated by a constant clearance. This method can be used for diameter ratios greater than 0.3 [7]. Recently, regression models were developed using experimental and theoretical studies conducted for concentric annulus [2-3]. Aqueous suspensions of PolyAnionic Cellulose (PAC) for PL fluids and Xanthan Gum (XG) for YPL fluids with different weight concentrations were utilized. Then, the narrow-slot approximation method results were utilized to fit a regression model. The proposed models showed a good agreement with experimental results. Erge *et al.* [4] modeled the flow equations during tripping operations numerically. The governing equation of motion of Herschel Bulkley fluid flow in a concentric annulus with a CEP is discretized using the finite difference method (FDM), then the resulting system of algebraic equations was solved numerically. On the other side, the CFD technique has known an important improvement which allows it to handle complicated problems in petroleum engineering, especially in drilling hydraulics [18-19].

Recently, Machine Learning (ML) becomes a very important tool for solving complicated problems, especially in the petroleum industry. In the presence of a significant amount of data, these algorithms proved to be a very powerful alternative to the classical physics-based methods. Razi *et al.* [20] used the Neural Networks algorithm to predict rheological properties of water-based drilling fluids. A good agreement was found between the model predictions and experimental data. Based on the same algorithm, Rooki [21] developed a ML algorithm to predict pressure losses for the flow of YPL fluid in concentric and eccentric annulus. Krishna *et al.* [22] developed an Artificial Neural Network (ANN) model to estimate surge and swab pressures in case of PL fluid during tripping operations using a wide range of drilling fluid and wellbore parameters values.

The aim of this paper is, firstly, to present new models to estimate steady-state surge pressures induced by the flow of non-Newtonian drilling fluids in a concentric annulus during tripping operations and, secondly, to study the influence of drilling parameters on surge (and swab) pressures. Hence, four different models were presented: a semi-analytical approach, two numerical models, and a surrogate model. Firstly, a new semi-analytical model was utilized where the flow equations are developed analytically then solved numerically (Appendix A). As compared to the existing models from the literature, this new model uses a different approach and introduces new additional constraints to the algorithm in order to ensure that non-physical solutions are ignored. Secondly, a new numerical model based on the FDM was established (Appendix B), this model was stable and showed a satisfactory agreement as compared with the results of other methods. Alternatively, the commercial package (Ansys-Fluent 19R3) was adopted to support the results found from the first and the second models. The results of these models are, then, validated using the published experimental measurements [3] and using existing models in the literature namely the narrow-slot technique which is considered the most popular method for modeling drilling hydraulics. Also, the developed models were successfully extended to model the PL fluid flow using very low yield stress values. The numerical model was used to perform an extensive parametric study which allows us to analyze the effect of the major influencing factors on the surge pressures namely: pipe velocity, annular geometry, and rheological parameters. Lastly, to investigate the effectiveness of the modern ML algorithms for solving drilling problems in general, and in modeling complex drilling fluid flows in particular, the outcome of the extensive parametric analysis is used as the basis for constructing a surrogate model using the Random Forest Regressor (RF) algorithm that correlates the surge pressure directly with the relevant drilling parameters. Once this model is well trained and tested, it can be used to calculate surge pressures directly without the need to perform cumbersome numerical calculations.

2. Materials and methods

2.1. Modeling assumptions

During tripping operations, the drill pipe is run in (or pulled off) the bottom hole, the moving drill string forces the drilling fluid to flow upwards (or downwards) through the annular space (Fig. 1). In the upcoming developments, the following assumptions are considered:

- The cylinders are completely vertical, sufficiently long so that fully developed flow would be established;
- The drilling fluid has a non-Newtonian behavior, single-phase, and incompressible;
- The flow is considered to be laminar and steady-state;
- The drill string is assumed to be completely closed-ended so that inertial effects are small and can be ignored [23].
- Only surge pressure is considered, however, the developed models can be used for the case of swabbing since they are similar phenomena.

The fluid flow between two concentric cylinders using the previous assumptions can be described by the following equation,

$$\frac{1}{r}\frac{d(r\tau)}{dr} = -\frac{dp}{dz} \quad (1)$$

where r is the radius, $\frac{dp}{dz}$ stands for pressure gradient and τ is the shear stress which is related to the shear rate ($\dot{\gamma}$) by a relationship of the form,

$$\tau = \mu(\dot{\gamma})\dot{\gamma} \quad (2)$$

in which μ is the apparent viscosity which depends on the shear rate for non-Newtonian fluids. Equation (1) is subject to the following boundary conditions,

$$v = \begin{cases} v_p, & for\ r = r_p \\ 0, & for\ r = r_h \end{cases} \quad (3)$$

where v_p is the drill pipe velocity (for surge pressure, $v_p < 0$ and for swab pressure, $v_p > 0$) with no slips at the walls.

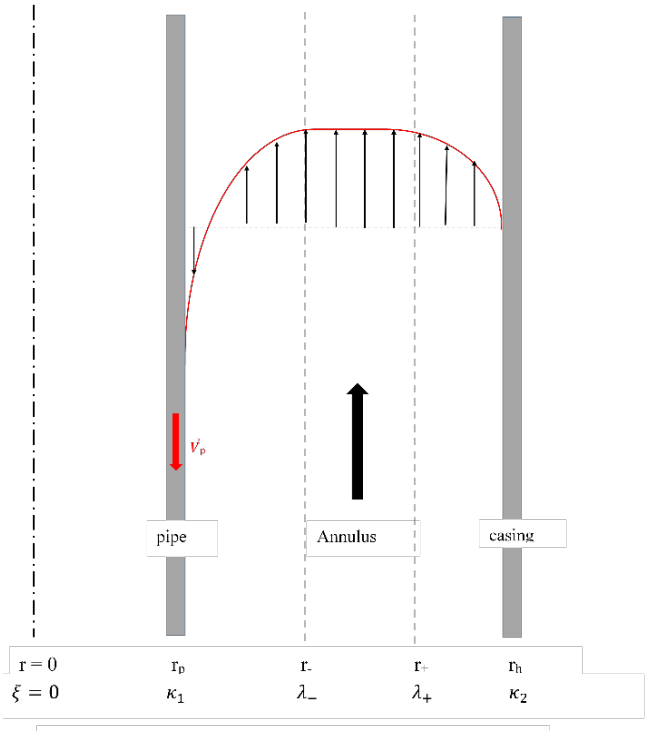

Fig. 1. Surge phenomenon in a concentric annuli

2.2. Rheological model

There are a lot of constitutive laws describing the rheological behavior of fluids. In the drilling industry, it is well known from the literature that Herschel-Bulkley rheological model best represents drilling fluids while modeling wellbore hydraulics [24]. Its constitutive law is given by,

$$\tau = \pm \tau_0 \pm K\left(\frac{dv}{dr}\right)^n \quad (4)$$

where τ_0 is the yield stress, n is the flow behavior index and K is the consistency index.

According to this law, the fluid has mainly two flow regions: a sheared region with a varying velocity and a plug region behaving like a solid with a constant velocity. The coexistence of these two flow regimes (plug and shear) with distinct internal boundaries that must be determined as part of the solution makes it very difficult to use, directly, CFD methods while describing these fluid flows. Even if the plug zone's size and shape are known, shear rate discontinuities at plug boundaries imply non-existent derivatives which may cause numerical instabilities. A solution to this problem was presented by [25] using a bi-viscosity model in which the apparent viscosity is taken to be constant with a high value (μ_{max}) if the shear rate falls below a pre-specified low level called the cut-off shear rate ($\dot{\gamma}_c$). The determination of the appropriate value for this ($\dot{\gamma}_c$) or (μ_{max}) is difficult. Above this threshold, the usual constitutive equation is used.

The constitutive model used in the developed numerical model in the upcoming studies is the one proposed by Mendes and Dutra [26] in Eq. (5), which is a single constitutive law that can be applied at any point in the flow domain and the internal boundaries do not need to be determined, the plug and sheared domains while solving the equations. Also, it is a continuous function that possesses continuous derivatives and automatically provides rapid transitions across the boundary separating plug and sheared flows. Therefore, standard numerical methods formulas can be easily applied [27].

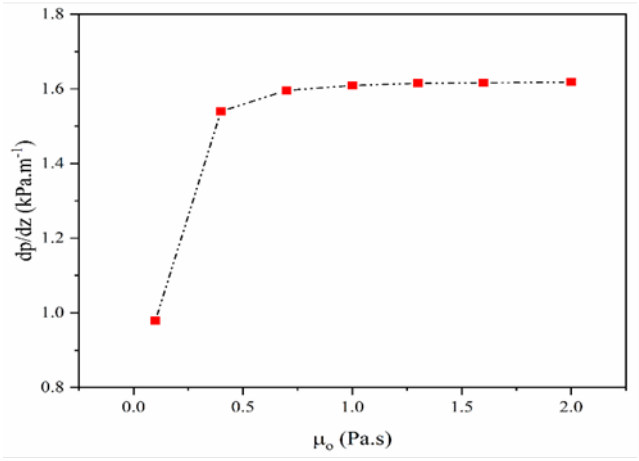

Fig. 2. Fluid velocity profile for different values of (μ_0)

The plug zone viscosity (μ_0) must be chosen wisely, high values can be chosen since they best represent high viscosities at the plug zone (similar to solids) to stabilize the numerical schemes, but not too high since higher values require an expensive computational cost to reach convergence [28]. To choose an optimal value for (μ_0), a sensitivity analysis was performed by plotting surge pressure gradient for different values of (μ_0) as demonstrated in Fig. 2. The pressure gradient slightly changes for values of (μ_0) bigger than 1 Pa.s, which means that the solution becomes almost independent of (μ_0) values. In this study, (μ_0) is taken to be 1 Pa.s.

$$\mu = \left(1 - exp^{-\mu_0 \frac{\dot{\gamma}}{\tau_0}}\right)\frac{(\tau_0 + K\,(\dot{\gamma})^n)}{\dot{\gamma}} \quad (5)$$

In the commercial solver Ansys-Fluent, a hybrid apparent viscosity has been used in order to overcome the discontinuity of viscosity at the plug zone [29]. Two separate viscosity models are used for the sheared and the plug regions where these two regions get distinguished by introducing a critical shear rate value ($\dot{\gamma}_c$) instead of zero.

When ($\dot{\gamma}$) is lower than ($\dot{\gamma}_c$),

$$\mu = \frac{\tau_0\left(2 - \frac{\dot{\gamma}}{\dot{\gamma}_c}\right)}{\dot{\gamma}_c} + K\left({\dot{\gamma}_c}^{n-1}\right)\left[(2-n) + (n-1)\frac{\dot{\gamma}}{\dot{\gamma}_c}\right] \quad (6)$$

When ($\dot{\gamma}$) is bigger than ($\dot{\gamma}_c$),

$$\mu = \frac{\tau_0}{\dot{\gamma}} + K(\dot{\gamma})^{n-1} \quad (7)$$

2.3. Surge models

While modeling YPL fluids in the annulus, the velocity profile exhibits three different zones: two sheared zones at the limits and a plug zone at the center. When tripping the pipe in, the fluid flows upwards, while in the region close to the moving inner wall, the fluid moves downwards with the pipe due to the no-slip assumption (the clinging effect) (Fig. 1). Based on the equation of momentum and mass conservation, the velocity profile at each flow region can be derived which will be, then, used to calculate the flow rate. The detailed mathematical derivations of the semi-analytical and numerical models are presented in (Appendix A) and (Appendix B), respectively.

Analytical solutions of laminar flow equations for YPL fluids in concentric pipes are not found in the open literature because the analytical integration of the equations for surge pressures not possible due to the non-linearity of the model. However, they do exist for some special cases, that is, either the geometry is approximated as a narrow slot, both walls are assumed to be stationary, or the rheology is reduced to Bingham plastic, PL, or Newtonian models. That justifies the use of semi-analytical models and numerical techniques to solve such problems.

2.4. Semi-analytical model

In semi-analytical models, the frictional pressure losses as a function of the flow rate are expressed analytically, but the quantitative solution depends on parameters that are given by integrals or implicit equations that must be solved numerically.

Haige and Xisheng [9] and He *et al.* [17] presented semi-analytical models that calculate surge and swab pressures gradient in a concentric annulus, in which the algorithm is an iterative solver that calculates numerically the analytical integrals for both velocity distribution and flow rate. In this paper, additional constraints are added which allow to avoid non-physical solutions during iterations. Chin [27] presented an exact semi-analytical approach to solve the flow of YPL fluids in fixed concentric pipes for CEP and stated the required constraints to ensure physical solutions. The same mathematical procedure is used in this model, but it is extended to the case of a moving pipe using dimensionless variables. The approach produces integral solutions in terms of a dimensionless parameter "C*", which satisfies some kinematic and dynamic constraints. This parameter is determined using an iterative procedure, then, the velocity profile is obtained based on this parameter (C*) which will be utilized to calculate the total volumetric flow rate. The boundary conditions in Eq. (3) are used.

This problem must be solved iteratively since the flowrate is pre-specified while the corresponding pressure loss is unknown. The procedure contains two loops: an inner and an outer loop. The inner loop solves the momentum equation, by updating the parameter "C*" iteratively, till a change of sign is occurred in Eq. (A-16). Then, that value of (C*) is used to evaluate the integrals to get the velocity profile. After that, in the outer loop, the volumetric flow rate is calculated based on this velocity profile and compared with the volumetric flow rate induced by the pipe movement. Mass conservation acts as a constraint and pressure gradient was updated using the secant's method till mass conservation is satisfied to a prespecified tolerance (ϵ_2). Mathematically, since the fluid is considered to be incompressible, the flow rate calculated in the outer loop (Q) must be equal ($\pm\epsilon_2$) to the flow caused by pipe movement (Q_p) (Eq. (A-23)).

The results are presented in terms of dimensionless surge pressure gradient and generalized Bingham number. The dimensionless surge pressure gradient is defined as,

$$P = -\frac{dp}{dz}\frac{D}{\tau_0} \quad (8)$$

The generalized Bingham number (the yield number) is defined as,

$$Bi = \frac{\tau_0}{K}\left(\frac{D}{|v_p|}\right)^n \quad (9)$$

The dimensionless stress can be written as,

$$T = P\left(\frac{\xi}{2}\right) + \left(\frac{C^*}{\xi}\right) \quad (10)$$

A code was implemented in Python 3.7 to compute the dimensionless surge pressure gradient for a given (Bi). The procedure is summarized in the following flowchart (Fig. 3). The development of the equations is presented in Appendix A.

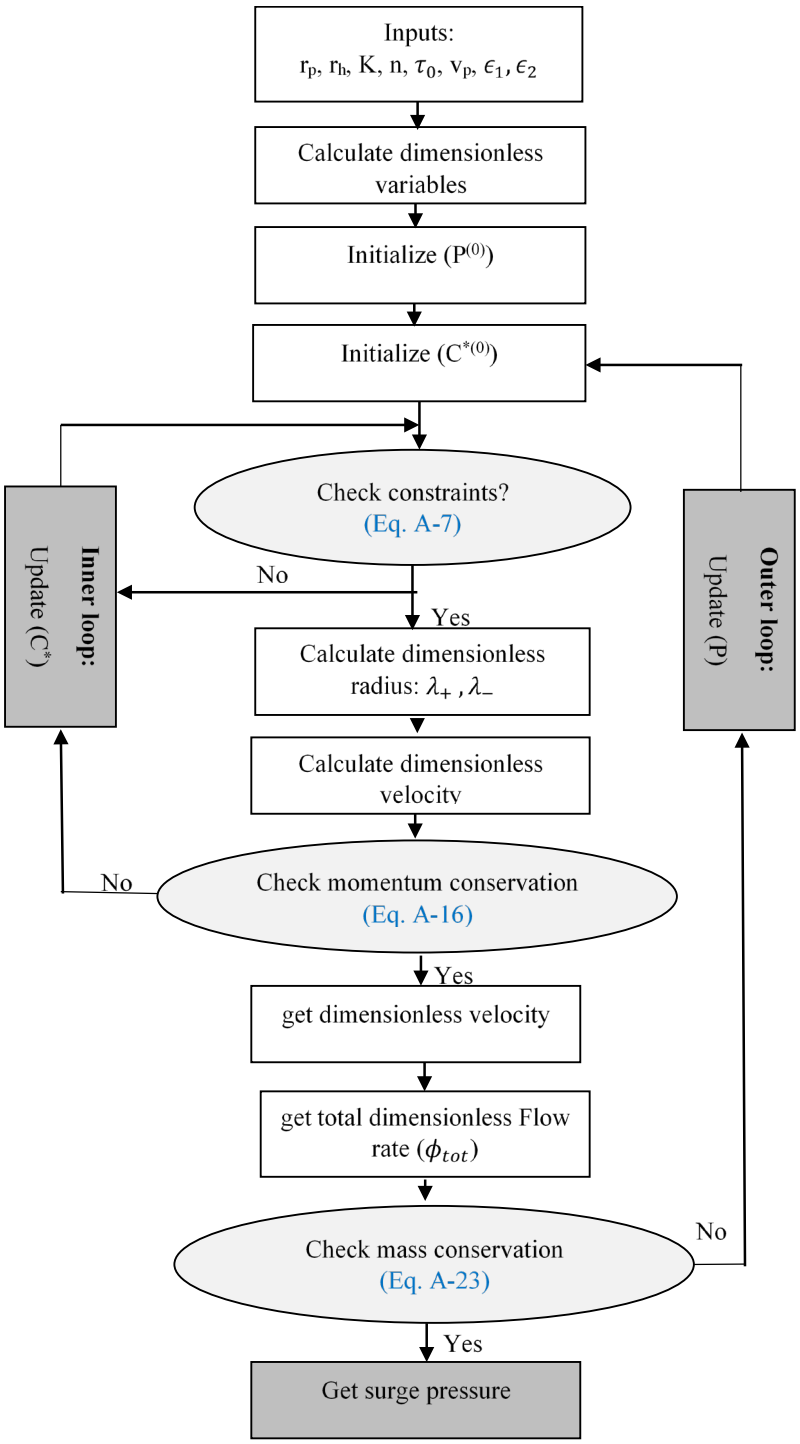

Fig. 3. Semi-Analytical model's algorithm

2.5. Numerical model

Numerical modeling provides the most powerful and innovative techniques for solving modern and complex engineering problems. In a concentric annulus, the problem is symmetric, so, there is no need to generate complicated mesh structures such as unstructured or body-fitted meshing. Thus, a simple one-dimensional numerical model would be sufficient. In this section, a numerical model for estimating surge pressure was introduced. The governing flow equation is discretized using the FDM, then it was solved using the Gauss-Seidel method. The discretized equation used in the numerical solution is given in Eq. (11). The mathematical derivation of the model and the coefficients A_p, A_n, A_s, and b_i are given in Appendix B.

$$A_p v_i + A_n v_{i+1} + A_s v_{i-1} = b_i \quad (11)$$

A second-order central differencing was used for all interior points. While first-order forward and backward differencing schemes were used for the inner and outer boundaries, respectively. Moreover, the inner and outer pipe walls are subject to the boundary conditions in Eq. (3).

Eq. (B-4) is a non-linear partial differential equation (PDE) and it is linearized during the discretization to get a system of linear algebraic equations (Eq. 11) which will be then, solved iteratively using the Gauss-Seidel method. The numerical procedure contains two loops: an inner and an outer loop. The inner loop solves the momentum equation where the non-linearity is handled by evaluating the source of the non-linearity (apparent viscosity) using velocity values from the previous iteration, which will be then, used to update the velocity values in the next inner loop iteration. This inner loop ends when the convergence criterion is satisfied, as follows,

$$\sum_i \left(\frac{\left(v_i^{k+1} - v_i^k\right)^2}{(v_i^k)^2} \right)^{\frac{1}{2}} < \epsilon_1 \quad (12)$$

where v_i^{k+1} and v_i^k are the velocity values at node (i) of two successive iterations $(k+1)$ and (k), respectively.

In the outer loop, the algorithm must satisfy the mass conservation which will be used as a constraint and the pressure gradient gets updated using the secant's method till mass conservation is satisfied to a pre-specified tolerance. Mathematically, this means that the flow rate calculated using the velocity values from the outer loop (Q) must be equal $(\pm\epsilon_2)$ to the flowrate caused by pipe movement (Q_p) (Eq. 13).

$$|Q - Q_p| < \epsilon \quad (13)$$

It would be better to use the relative error instead of the absolute error in Eq. (13) because in this case, it is easier to choose the threshold (ϵ_2) to judge the accuracy of the model and how well the mass conservation equation is conserved (Eq. 14).

$$\frac{|Q - Q_p|}{Q_p} < \epsilon_2 \quad (14)$$

The flow chart in Fig. 4 summarizes the numerical procedure, where the subscripts (k) and (m) denote the number of inner and outer iterations, respectively. A code is written in Python 3.7 to calculate surge pressure using this numerical procedure.

A grid sensitivity analysis was performed to choose the best number of radial grid points to ensure that the model results are grid-independent, that is, an increase in grid points does not improve the mathematical solution. For all scenarios used in this paper, the number of radial grid points equals to (n_g=40) is proved to be sufficient since the surge pressure gradient becomes almost independent of the grid points for (n_g>40). Hence, the use of a higher number of grid points would not improve that much the accuracy, but, it will increase the time and cost, only (Fig. 5).

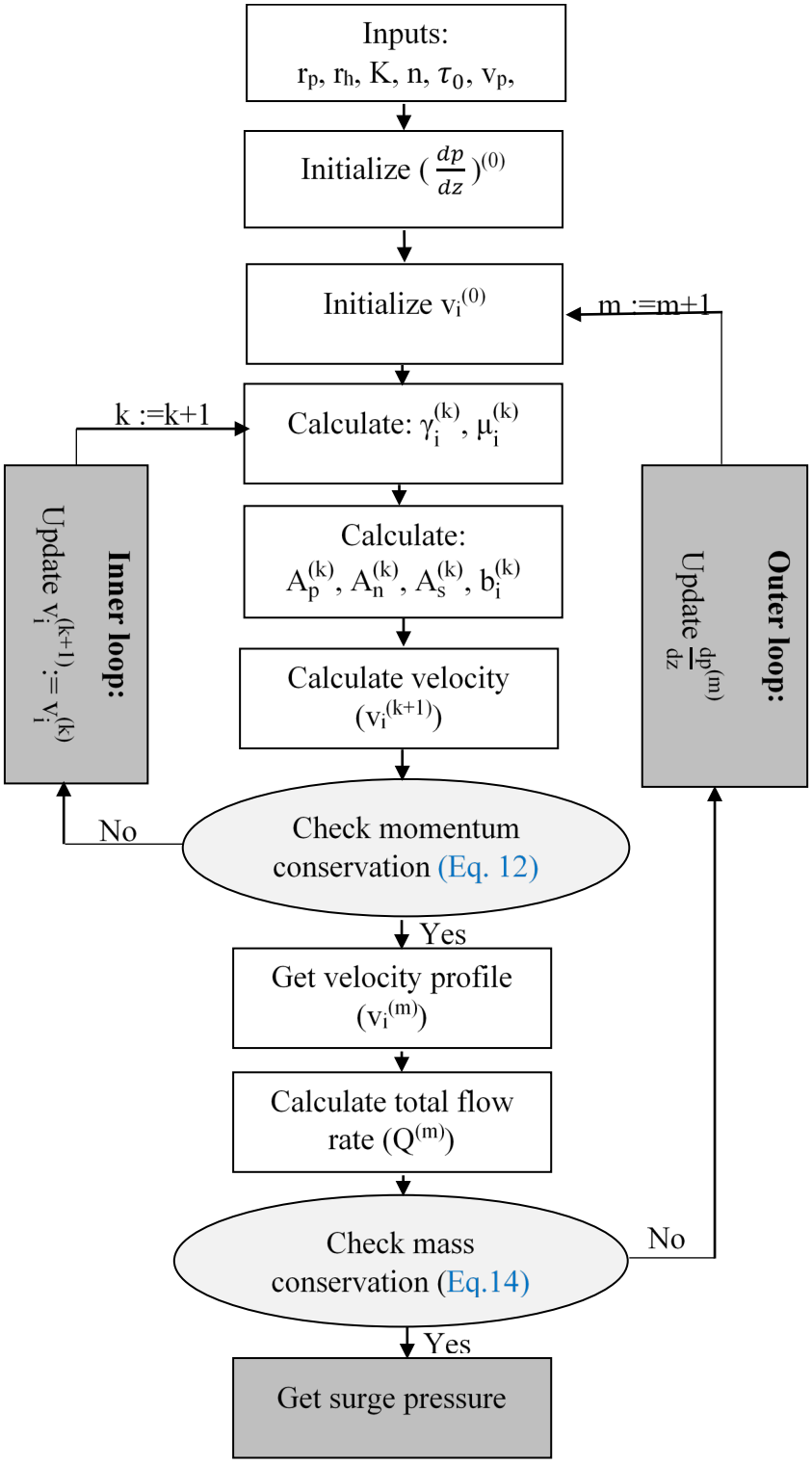

Fig. 4. Numerical model's algorithm

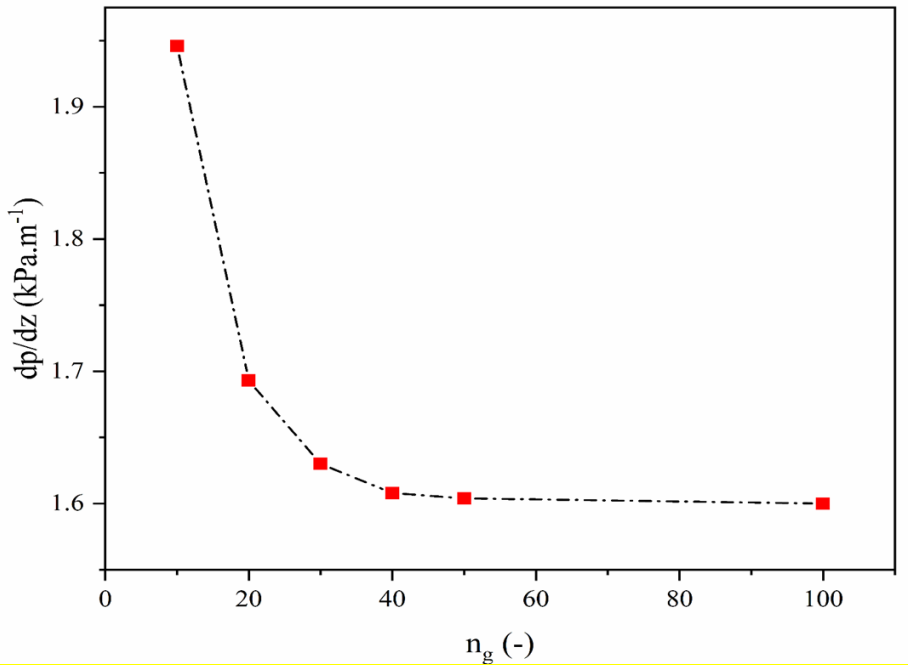

Fig. 5. Grid points sensitivity for the numerical model

2.6. Commercial software Ansys-Fluent

CFD is the field of science that integrates and combines the disciplines of fluid mechanics and heat transfer with both mathematics and computer science. With the recent progress in computer science, CFD has not only become one of the three basic methods for solving complicated engineering problems in fluid dynamics and heat transfer along with experimental and analytical approaches, but it is expected to become at the forefront of cutting-edge research in fluid dynamics [30]. That is why, in recent years, engineers have become more interested in the use of the most recent commercial CFD codes such as ANSYS Fluent.

In this paper, the commercial CFD software, ANSYS Fluent 19R3, was used to model drilling fluid flow through the annulus while moving the inner pipe downwards. Hexahedral meshes are used as the base mesh type in the annular geometry. To take into account the high-velocity gradients in the boundary layer near the walls, a refined mesh near the walls is adopted since in this case, the inner wall moves with a certain velocity. While a coarse mesh is considered in the middle of the annulus, which would make the simulations more stable and accurate. A grid sensitivity study is conducted to determine up to what extent the mesh needs to be refined to get an acceptable level of tolerance, in order to make sure that Ansys Fluent results are independent of grid size. Consequently, the lowest possible grid size is kept to both reduce the calculation cost and maintain the accuracy of the solution. Ansys Fluent solution is less sensitive to the grid size in the azimuthal direction than it is to the radial direction [28]. For that, during grid sensitivity analysis, higher interest was taken in the radial direction. In this study, grid sensitivity analysis showed that Ansys Fluent results become independent from the adopted grid size when a grid number of (30×100) is employed (Fig. 6). The "pressure-based" solver was used in which the momentum equation was used to obtain the velocity profile, while, the pressure profile was obtained by solving a pressure correction equation which was derived by combining mass and momentum equations. Since drilling fluid flows through annuli are governed by nonlinear and coupled equations, momentum and mass conservation equations are solved numerically using an iterative scheme till the residual errors are minimized to a pre-specified threshold. During these simulations, the max residual error was 0.001%. The "SIMPLE" was used as the solution algorithm where the governing equation is solved sequentially [29].

Boundary conditions in Eq. (3) are applied to the inner and outer walls. A specified velocity and pressure boundary conditions are used at the inlet and outlet, respectively. The specified velocity at the inlet is related to the pipe velocity, pipe, and hole diameters so that mass is conserved (Eq. 15).

$$v_{inlet} = -\left(\frac{1}{\left(\frac{r_h}{r_p}\right)^2 - 1}\right) v_p \tag{15}$$

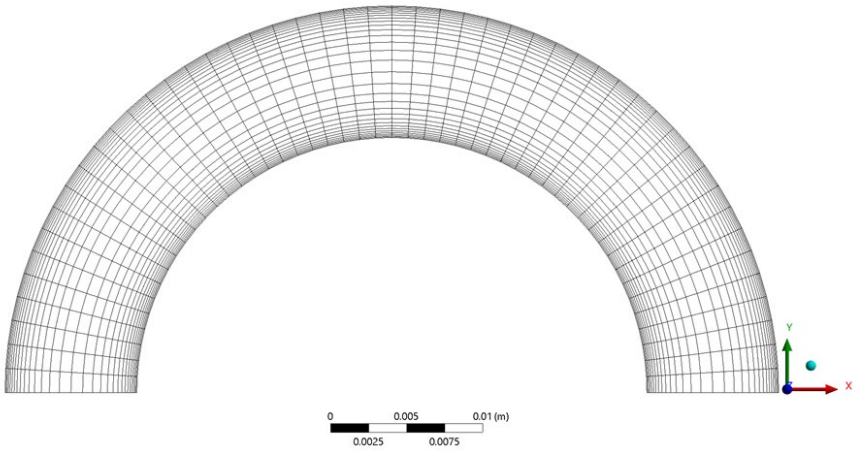

Fig. 6 Mesh cross-section of the concentric annulus

2.7. Surrogate model

In this part, the performance of ML algorithms in the modeling of drilling fluid flows during tripping operations is assessed, since the surrogate models resulting from these algorithms can be a powerful alternative to the classical numerical and analytical models. Modeling these fluid flows on the drilling site is almost impossible, and even if it is possible, the limitations of the narrow-slot approximation and the high cost of semi-analytical and numerical models which require cumbersome numerical calculations whenever the parameters are changed make this task very challenging. For that, surrogate models are introduced and once they are fully trained and well tested, they can be used, directly, to predict surge

pressures. Thus, these models have two main characteristics: they mimic the behavior of the simulations as closely as possible and they are completely cheap to evaluate.

A wide range of pipe and hole radius, fluid rheology properties, and pipe velocities (Table 1) have been used to perform an extensive parametric study based on the previously developed numerical model, then, a RF Regression model is fully trained using the input parameters which are picked based on the sensitivity analysis. In this case, pipe and hole radius, yield stress, index behavior, consistency factor, and pipe velocity are the input parameters while pressure gradient is the output. To ensure generalization, the performance of the trained model must be well tested against new scenarios. A total of 19800 data points are collected, 70% was used as the training set, while the remaining 30% was used for testing the trained model. Table 1 shows the range of the data used in this study.

In the current study, an ensemble ML algorithm was used. This type of model is considered to be a black box for which the model parameters do not have any physical significance in terms of equivalence to the real physical parameters. RF is an ensemble ML algorithm used for nonlinear multiple regression and classification problems. It trains multiple decision trees in parallel, each tree gives an output, then uses averaging, so that the predictive accuracy is improved and the overfitting problem is easily controlled [31]. The number of trees and estimators are the algorithm's hyper-parameters that need to be tuned in order to construct a

generalized model whose predictions are independent of its own hyper-parameters. To do so, the algorithm was generated using different decision trees and estimators' number, then, the testing R2-score was computed for each scenario. As long as an increase in the number of trees and estimators do not improve the value of this R2-score, that number of trees and estimators is used to generate the model. Decision trees are typically more suited towards classification problems and when used for regression, the results are very much stair-stepped. This issue was mitigated by using a very high number of data.

Table 1. Range of input data

Parameter	Min.	Max.	Average
Hole radius (m)	0.1	0.2	0.151
Radius ratio (r_p/r_h)	0.2	0.8	0.473
K (Pa. s^n)	0.5	3	1.717
n	0.5	0.9	0.692
τ_0 (Pa)	1	11	6.005
v_p ($m.s^{-1}$)	-0.1	-0.9	-0.489

The algorithm is implemented in Python 3.7 using Scikit-Learn which is a Python library containing a variety of ML algorithms for supervised and unsupervised problems [32]. Once fully trained, the generated model is stored in the software library and can be easily reused.

3. Results and discussion

3.1. Model validation

To assess the performance of the developed models, dimensionless surge pressure gradient (P) was computed for different dimensionless Bingham number (Bi), then, compared with the theoretical and experimental results from previously published studies. The used geometry parameters and fluid properties are given in Table 2. Two different Herschel Bulkley fluids were obtained from the study of Crespo and Ahmed [3] were used for validation. Figure 7 and Figure 8 show that the developed models predict the experimental surge pressure gradients results with good accuracy. Moreover, the relative error is computed for each model using Eq. (16).

$$E_r = \frac{|P_{experimental} - P_{model}|}{|P_{experimental}|} \quad (16)$$

The narrow-slot approximation is the most used method for solving drilling hydraulics problems, where this method approximates the annular flow using the equations developed for flows through rectangular slots. It is much simpler than the other methods and provides accurate solutions for diameter ratios greater than 0.3 [23].

3.1.1. Validation of the semi-analytical model

In the developed semi-analytical model, while iterating, the constraints in Eq. (A-7) were checked to ensure that the solution is physically acceptable. The algorithm was stable and converges to the desired solution. On the other hand, the value of the relative error (ϵ_2) is taken to be equal to (10^{-3}). Comparison of the results of the semi-analytical model with other results is shown in Fig. 7-a and Fig. 7-b. For HB-I, the semi-analytical results show a good coincidence with both experimental data and narrow-slot approximation results. The average relative error was ±2.5% and ±1% for the semi-analytical model and the narrow slot, respectively. For HB-II, the semi-analytical model shows an average relative error of ±7.8 %, while the average relative error for narrow-slot approximation is ±8.2 %.

3.1.2. Validation of the numerical model

After performing a grid sensitivity analysis, 40 radial grid points were used while generating the new numerical model. The model was stable and gives accurate results where a value of (10^{-2}) is considered for the relative errors (ϵ_1) and (ϵ_2). In Fig. 7-a and Fig. 7-b, the solutions collected from the numerical model are presented. For HB-I, the average relative error for

the numerical model was ±2.9%, while it was ±1% using the narrow-slot approximation. For HB-II, an average relative error of ±3.5% was reported when the numerical model was compared to the experimental data, while this error was estimated at ±8.2% when the narrow-slot approximation was used.

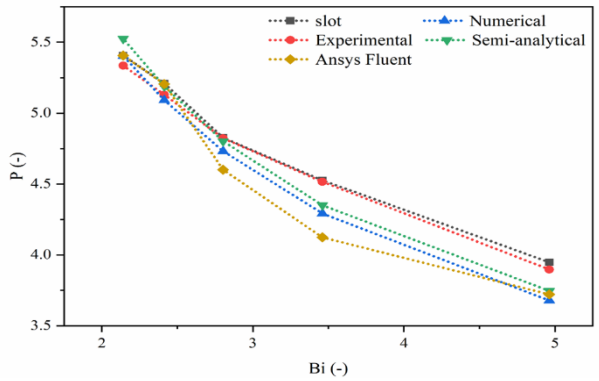

Fig. 7-a Comparison between the developed models, Ansys-Fluent, slot results, and experimental data (HB-I)

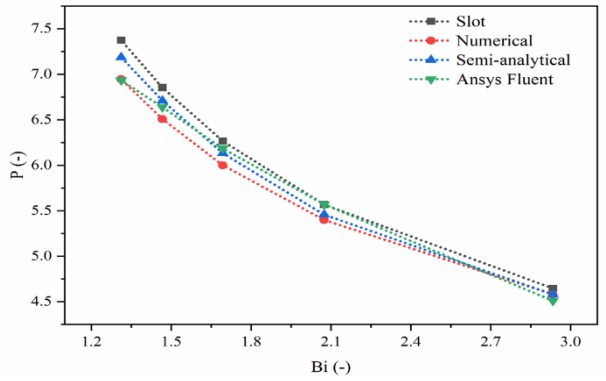

Fig. 7-b Comparison between the developed models, Ansys-Fluent, slot results, and experimental data (HB-II)

3.1.3. Validation of Ansys Fluent

Ansys-Fluent 19R3 was used to construct a CFD model capable of predicting surge pressure in the annular space. After meshing and implementing the corresponding boundary conditions of the problem, the resulting model was used to conduct the different scenarios in Table 2. Then, the results were compared with the others models results, as exhibited in Fig. 7-a and Fig. 7-b. For both HB-I and HB-II, Ansys Fluent model shows good matching with an average relative error of ±4 % and ±5%, respectively. This justifies the power of using CFD tools for modeling complicated drilling fluid flows.

Table 2. Experimental data for Herschel Bulkley fluids [3]

	τ_0 (Pa)	K (Pa.s^n)	n (-)	Pipe radius (mm)	Hole radius (mm)
Herschel Bulkley I (HB-I)	3.44	0.359	0.52	16.75	25.4
Herschel Bulkley II (HB-II)	7.8	0.553	0.5	16.75	25.4

The experimental results presented by Crespo and Ahmed [3] were limited to low velocities (less than 0.21 m.s^{-1}). This is because longer stroke lengths are required to reach the steady-state condition in case of higher velocities.

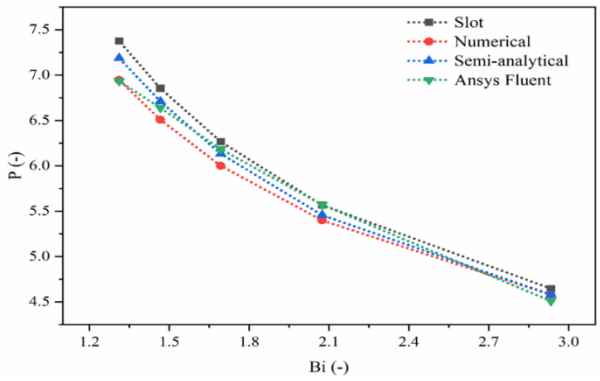

Fig. 8. Comparison between the developed models, Ansys-Fluent, and slot model results for high velocities (HB-II)

Due to lack of experimental data, the performance of the developed semi-analytical, numerical, and Ansys Fluent models in case of high tripping velocity values were assessed using the slot-approximation model as long as the diameter ratio is bigger than 0.3 (0.66 in this study) where the narrow-slot technique is expected to give accurate results. A range of pipe velocities between (0.2 m.s^{-1} and 1 m.s^{-1}) was considered, as shown in Fig. 8. The developed models and the narrow-slot approximation results are in acceptable agreement. So, all developed models can be used for predicting surge pressure while tripping operations with con-

fidence, even for higher velocities that were experimentally unrealizable. This proves the use of mathematical models as a powerful predictive tool while studying experimentally difficult or unrealizable conditions.

3.2. Extension of the developed models to PL fluids

Although the YPL model usually gives the best fit for the rheological measured data as compared to other rheological models for drilling fluids, a lot of drilling fluids' rheological behavior was proved to be best represented by the PL model. A lot of studies were conducted in the literature using this theological model for studying different drilling fluid flow problems [6-7]. To assess the adaptability of the developed numerical and semi-analytical models, they are extended to the case of PL fluid models. The same procedure used for the YPL shown in Fig. 3 and Fig. 4 is used for the PL model where the only difference is the value of the yield stress since the PL fluids do not exhibit yielding stress. In this study, a very low value of (τ_0) was used (10^{-5} Pa). The experimental data (Table 3) presents two different fluids with rheological behavior of PL model, the experimental data published by Crespo and Ahmed [3] are used for comparison. Schuh model [6] is also utilized for comparison purposes since it is considered to be an accurate numerical model for predicting steady-state PL fluid flows in the concentric annulus.

Table 3. Experimental data for PL fluids [1]

	K (Pa.s^n)	n (-)	Pipe radius (mm)	Hole radius (mm)
0.28%PAC and 0.22%XG (PL-I)	0.774	0.5	16.75	25.4
0.75% PAC (PL-II)	0.670	0.67	16.75	25.4

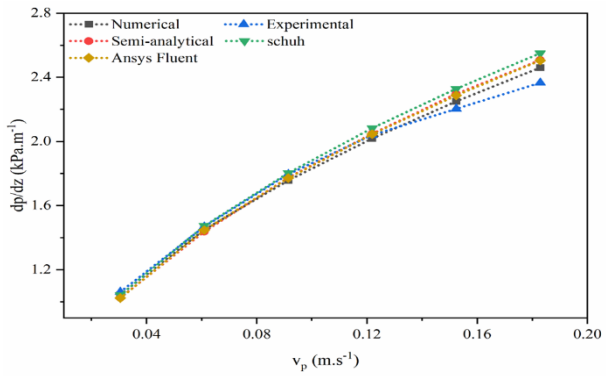

Fig. 9-a Comparison between the developed models, Schuh, and the experimental results for (PL-I)

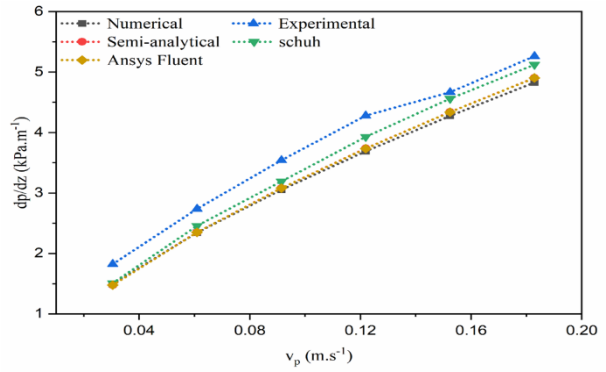

Fig.9-b Comparison between the developed models, Schuh, and the experimental results for (PL-II)

The results for the first PL fluid (PL-I) are presented in Fig. 9-a. As can be observed, the developed models show a reasonable agreement with the experimental and Schuh results. However, with the increase of velocity, the discrepancy with experimental data increases. The average relative error is estimated at ±2% for the numerical model, while, an average relative error of ±2.6% is found for Ansys Fluent and semi-analytical models and ±3% for the Schuh model. Fig. 9-b shows a comparison between the different models with the experimental data for the (PL-II), in which the results were less accurate than those for (PL-I), and the model of Schuh outperform the new models. Moreover, the average relative error was ±12% and 8.4% for the developed models and Schuh models, respectively.

3.3. Sensitivity analysis

After validating the developed models, parametric analysis was conducted to examine the influence of the different parameters on surge pressure by monitoring the relationship between surge pressure gradient and pipe velocity while varying other drilling parameters. Using

the developed numerical model, the sensitivity of the surge pressure to fluid rheological parameters and borehole geometry was investigated. The base case input parameters for this analysis are $n = 0.5$, $K = 0.6$ Pa.s^n, $\tau_0 = 6$ Pa, $r_p = 0.0635$ m and $r_h = 0.136$ m. Figures 12, 13, 14 ,15 and 16 show the effect of fluid behavior index, yield stress, consistency factor, pipe radius and hole radius on surge pressure under different pipe velocity values. These figures show that the pipe velocity increase causes an increment of surge pressure independently of the parameter of interest as both annular flow velocity and wall shear stress increase, but, the rate of increase changes from one parameter to another. Also, for the same pipe movement velocity, the increase of the different rheological parameters causes a raise of the surge pressure with different rate of increase. High values of rheological parameters magnify the piston-cylinder effect resulting from tripping pipe which cause higher surge pressures.

The effect of the fluid behavior index on surge pressure is shown in Fig. 10. For the same value of flow behavior index, as pipe velocity increases, the surge pressure increases non-linearly and this increment is higher for high (n) values. On the other hand, the increment of the pipe movement velocity induces a slight effect on surge pressure for low values of the flow behavior index. Under the same pipe velocity, the increase of (n) values causes a non-linear increment of surge pressure with an increasing rate as the plug zone thickness and fluid thinning ability is enhanced.

Figure 11 shows a non-linear effect of yield stress on surge pressure drop under different pipe velocity values. For instance, under the same pipe movement velocity, the surge pressure increases with a decreasing rate as yield stress increases but this increase becomes less sensitive in the case of low velocities. Furthermore, under the same yield stress, the surge pressure increases with the increase of pipe movement velocity and it becomes more sensitive to pipe movement velocity as the yield stress increases since plug zone thickness and fluid's thinning ability are increased.

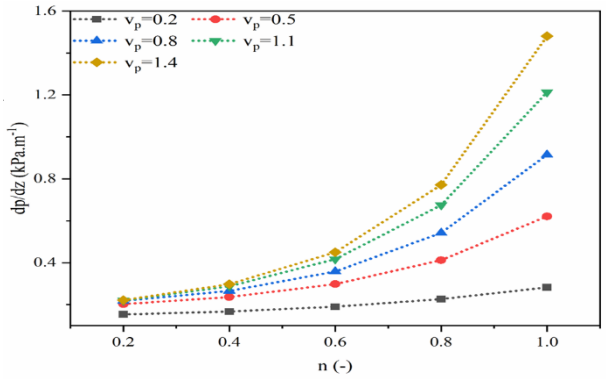

Fig. 10 Surge pressure gradient vs. fluid index behavior for different pipe movement velocities

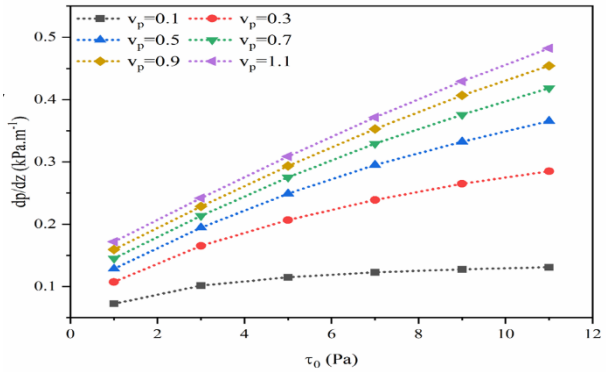

Fig. 11 Surge pressure gradient vs. fluid yield stress for different pipe movement velocities

Figure 12 indicates an almost linear relationship between the fluid consistency factor and the surge pressure for all considered pipe movement velocities. Moreover, the increase of the pipe movement velocity results in an increase of the surge pressure, and this effect is enhanced as the fluid consistency factor raises.

Additionally, the surge pressure increases with the increase of the pipe radius (or the decrease of the hole radius) as exemplified in Fig. 13 and Fig. 14. The increase of the pipe radius while keeping the hole radius fixed (or the decrease of the hole radius while keeping the pipe radius fixed) provides a smaller passage area for the drilling fluid (smaller annular clearance) which causes an increase in the drilling fluid flow rate being displaced resulting in higher surge pressures. This increase is also induced by the interaction of the fluid with annular walls when the ratio of diameters increases. Besides, the sensitivity of the surge pressure to pipe velocity increases with the increment of the pipe radius (or the decrease of hole radius).

Therefore, to avoid problems such as formation fracturing and kicks, the piston-cylinder effect must be reduced either by decreasing the relevant rheological parameters namely: yield

stress, fluid index behavior, and fluid consistency factor, decreasing drill pipe velocity, or increasing the annular clearance (either by increasing hole diameter or decreasing pipe diameter).

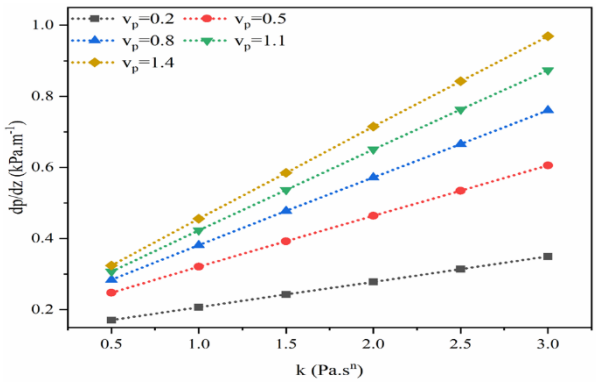

Fig. 12. Surge pressure gradient vs. fluid consistency factor for different pipe movement velocities

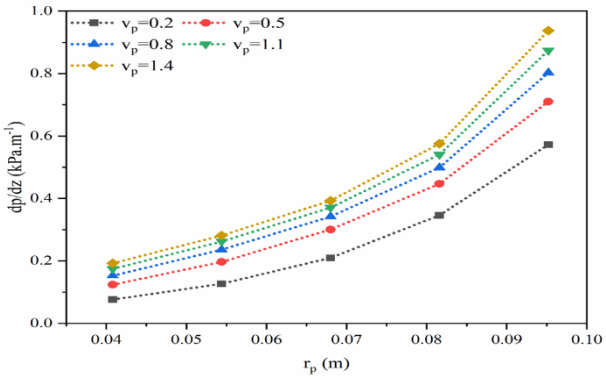

Fig. 13. Surge pressure gradient vs. pipe radius for different pipe movement velocities

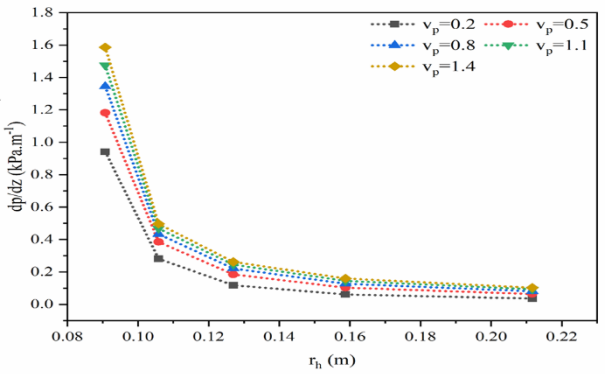

Fig. 14. Surge pressure gradient vs. hole radius for different pipe movement velocities

3.4. Surrogate model

Based on the outcome of the sensitivity analysis and the numerical model, a lot of simulations were conducted in order to generate a surrogate model. The sensitivity analysis gives the parameters of interest that affect the surge pressure, namely, the rheological properties, the annular geometry, and pipe velocity which serve as the inputs to the surrogate model. While the numerical model was used to generate 19800 simulation scenarios based on a wide range of values of these input parameters (Table 1). A RF algorithm was used to generate a surrogate model based on this set of data. This model was capable to predict surge pressure gradient in the concentric annulus with CEP.

After tuning the models hyper parameters using the Kfold cross-validation, 20 decision trees with 40 estimators were used as the RF algorithm architecture. The resulting training and testing data are plotted in Fig. 15-a and Fig. 15-b, in which the scatter plots show that the predicted surge pressures using the RF algorithm for both data sets fit very well the numerical results. Most of the RF predictions fall between ±10% and ±15% error bars for the training data set and testing data set, respectively. The calculated mean absolute error and Root-mean-square deviation for training data are 31.38 Pa.m^{-1} and 78.01 Pa.m^{-1}, respectively, with an R^2 of 0.998, whereas, the mean absolute error and Root-mean-square deviation are 75.9 Pa.m^{-1} and 205.15 Pa.m^{-1}, respectively, with an R^2 of 0.99 for testing data. High R^2 values of the training and test data sets indicate that the RF model is well trained and it is generalized so that it can be used to predict new scenarios with high accuracy. However, a slight distortion away from the best fit line is observed for the testing dataset for surge pressure gradients higher than 9 kPa.m^{-1}.

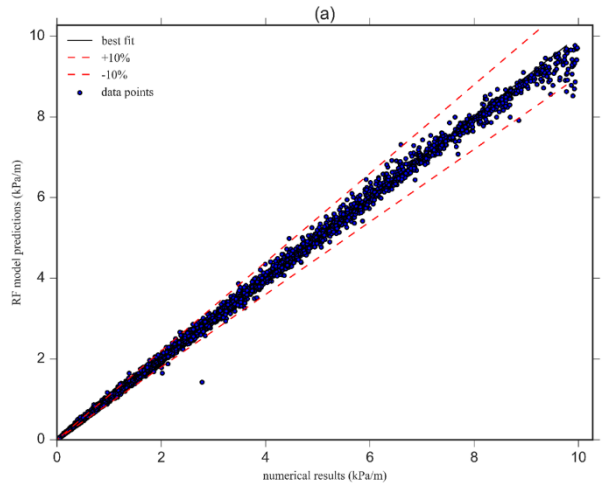

Fig. 15-a Comparison between numerical results and RF predictions for training data.

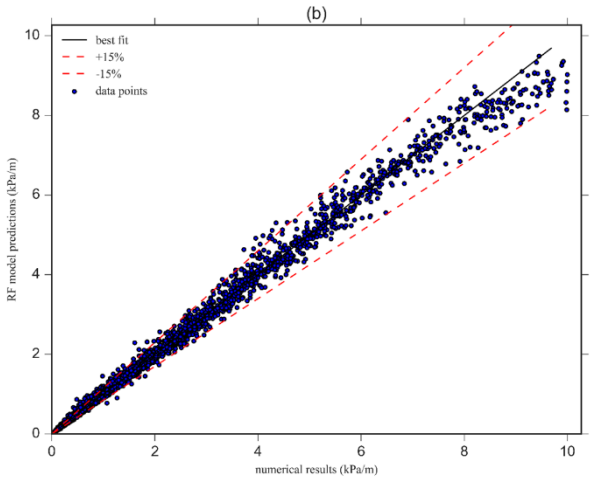

Fig. 15-b Comparison between numerical results and RF predictions for test data.

4. Conclusions

In this paper, new models for predicting surge pressure resulting from YPL fluid flows in a concentric annulus are presented, then, the effect of the different drilling parameters was studied.

- The developed semi-analytical model is stable and it predicts the surge pressure accurately. As compared to the existing models in the literature, the procedure used in this model is new and guarantees physical solutions by imposing new dynamic and kinematic constraints.
- The developed numerical model was stable and provides satisfactory results as compared to the experimental data taken from the literature.
- The results of ANSYS Fluent model were close to those of the other models indicating the efficiency of using CFD packages for solving drilling problems, especially fluid-related problems.
- The increase of the pipe movement velocity causes an increment of the surge pressure independently of the parameter of interest. But, the rate of increase changes from one parameter to another. Additionally, the effect of the pipe movement velocity diminished for small values of the rheological parameters or high annular clearances.
- To mitigate tripping-related problems, the piston-cylinder effect must be reduced either by decreasing the relevant rheological parameters, decreasing drill pipe velocity, or increasing the annular clearance.
- The RF algorithm was trained and tested based on numerical results where this surrogate model was capable of predicting surge pressure without the need for expensive numerical calculations. Moreover, the scatter plot shows a reasonable agreement between the RF predictions and the numerical results with an R^2 higher than 0.99 for both training and test data.
- The surrogate models can be considered as a powerful alternative method for solving complicated problems in the drilling industry.

Nomenclature

r	*Radius, m*	ξ	*Dimensionless radius*
r_p	*Pipe radius, m*	κ_1	*Dimensionless pipe radius*
r_h	*Hole radius, m*	κ_2	*Dimensionless hole radius*
D	*Annular clearance (r_h-r_p), m*	λ_+	*Dimensionless outer boundary limit of plug zone*
r_-	*Inner boundary limit of plug zone, m*	λ_-	*Dimensionless inner boundary limit of plug zone*
	outer boundary limit of plug zone, m	T	*Dimensionless shear stress*
r_+	*shear stress, Pa*		
	Fluid index factor.		

τ	*Consistency factor, Pa.s^n*	T_0	*Dimensionless yield shear stress*
n	*yield shear stress, Pa*	*P*	*Dimensionless surge pressure*
K	*pressure, Pa*	*Bi*	*Bingham number*
τ_0	*surge pressure gradient, Pa.m^{-1}*	ϕ	*Dimensionless total volumetric flow rate*
p	*z-coordinate, m*		
dp/dz	*viscosity, Pa.s*	ϕ_p	*Dimensionless volumetric pipe flow rate*
z	*plug zone viscosity, Pa.s*		***Acronyms***
μ	*shear rate, s^{-1}*		
μ_0, μ_{max}	*critical shear rate, s^{-1}*	*CEP*	*Closed Ended Pipe*
γ	*velocity, m. s^{-1}*	*OEP*	*Open Ended Pipe*
γ_c	*pipe velocity, m. s^{-1}*	*CFD*	*Computational Fluid Dynamics*
v	*total volumetric flow rate, m^3.s^{-1}*	*RF*	*Random Forest*
v_p	*pipe volumetric flow rate, m^3.s^{-1}*	*ML*	*Machine Learning*
Q	*relative error*	*YPL*	*Yield Power Law*
Q_p	*dummy variable*	*PL*	*Power Law*
Er	*grid point index*	*PDE*	*Partial Differential Equation*
x	*inner loop iterations index*	R^2	*Coefficient of determination*
i	*outer loop iterations index*	*NPT*	*Non Productive Time*
k	*number of grid points*	*FDM*	*Finite Difference Method*
m		*ANN*	*Artificial Neural Networks*
n_g			

Appendix A: Semi-analytical model

The force balance on a fluid element flowing in the annular space can be written as,

$$\frac{1}{r}\frac{d(r\tau)}{dr} = -\frac{dp}{dz} \qquad \text{A-1}$$

Then, the stress distribution can be expressed as,

$$\tau(r) = -\frac{dp}{dz}\frac{r}{2} + \frac{c}{r} \qquad \text{A-2}$$

In this paper, the effect of pipe movement on of Herschel-Bulkley fluid flow was studied, so, yield stress (τ_0), the pipe velocity ($|v_p|$) and the annular space ($D = r_h - r_p$) are used as the scaling parameters to make the system dimensionless.

$$T = \frac{\tau}{\tau_0}, \quad u = \frac{v}{|v_p|}, \quad \xi = \frac{r}{D}, \quad \kappa_1 = \frac{r_p}{D}, \quad \kappa_2 = \frac{r_h}{D} \qquad \text{A-3}$$

Equation (A-2) can be rewritten in dimensionless form as,

$$T = \left(-\frac{dp}{dz}\frac{D}{\tau_0}\right)\frac{\xi}{2} + \left(\frac{c}{D\tau_0}\right)\frac{1}{\xi} \qquad \text{A-4}$$

$$T = P\frac{\xi}{2} + \frac{C^*}{\xi} \qquad \text{A-5}$$

The dimensionless pressure gradient and the dimensionless parameter (C^*) are given, respectively, by,

$$P = \left(-\frac{dp}{dz}\frac{D}{\tau_0}\right)$$

$$C^* = \left(\frac{c}{D\tau_0}\right) \qquad \text{A-6}$$

The non-zero dimensionless parameter (C*) plays a key role in the analysis and must be chosen so that the following physical constraints must be satisfied,

$$C^* \leq \frac{1}{2|P|}$$

$$C^* \geq \frac{-P}{2}{\kappa_2}^2 \qquad \text{A-7}$$

$$\lambda_- > \kappa_1$$

$$\lambda_+ > \kappa_2$$

Where, $\lambda_-$and λ_+ are the dimensionless inner and the outer plug radius, respectively, which are given by the following expressions,

$$\begin{cases} \lambda_+ = \frac{1}{P}\left[1+\sqrt{1-2C^*P}\right] \\ \lambda_- = \frac{1}{P}\left[-1+\sqrt{1-2C^*P}\right] \end{cases} \quad \text{A-8}$$

Velocity profile

For the inner region $\boldsymbol{\kappa_1 < \xi < \lambda_-}$:

$$-\tau = \tau_0 + K\left(\frac{dv}{dr}\right)^n \quad \text{A-9}$$

In dimensionless form,

$$-T = 1 + \frac{1}{B_i}\left(\frac{du}{d\xi}\right)^n \quad \text{A-10}$$

Substituting Eq. (A-10) into Eq. (A-5), the dimensionless velocity profile is obtained, as follows,

$$u_I(\xi) = (B_i)^{\frac{1}{n}} \int_{\kappa_1}^{\xi} \left(-P\frac{x}{2} - \frac{C^*}{x} - 1\right)^{\frac{1}{n}} dx - 1 \quad \text{A-11}$$

where (x) is a dimensionless dummy variable.

For the outer region $\boldsymbol{\lambda_+ < \xi < \kappa_2}$:

$$\tau = \tau_0 + K\left(-\frac{dv}{dr}\right)^n \quad \text{A-12}$$

In dimensionless form,

$$T = 1 + \frac{1}{B_i}\left(-\frac{du}{d\xi}\right)^n \quad \text{A-13}$$

Substituting Eq. (A-13) into Eq. (A-5), the dimensionless velocity profile is obtained, as follows,

$$u_{III}(\xi) = (B_i)^{\frac{1}{n}} \int_{\xi}^{\kappa_2} \left(P\frac{x}{2} + \frac{C^*}{x} - 1\right)^{\frac{1}{n}} dx \quad \text{A-14}$$

For the plug region $\boldsymbol{\lambda_- < \xi < \lambda_+}$:

$$u_{II}(\xi) = u_I(\xi = \lambda_-) = u_{III}(\xi = \lambda_+) \quad \text{A-15}$$

Since the plug moves at a constant velocity, Eq. (A-15) can be used as a condition to ensure momentum conservation, that is, when the following condition is satisfied,

$$\epsilon_1 = [u_I(\xi = \lambda_-) - u_{III}(\xi = \lambda_+)] \quad \text{A-16}$$

While iterating, if two successive values of (ϵ_1) are of different signs, the algorithm is stopped and that value of (C^*) is considered, which will be used to get the velocity profile.

Flow rate

The dimensionless flow rate is given by the following equation,

$$\phi = \frac{Q}{2\,\pi\,|v_p|\,D^2} = \int u\,\xi\,d\xi \quad \text{A-17}$$

The dimensionless pipe flow rate is expressed using the following equation,

$$\phi_{pipe} = \frac{Q_p}{2\,\pi\,|v_p|\,D^2} = \frac{1}{2}\,\kappa_1^2 \quad \text{A-18}$$

For the inner region $\boldsymbol{\kappa_1 < \xi < \lambda_-}$:

$$\phi_1 = \int_{\kappa_1}^{\lambda_-} u_I(\xi)\,\xi\,d\xi \quad \text{A-19}$$

For the outer region $\boldsymbol{\lambda_+ < \xi < \kappa_2}$:

$$\phi_{III} = \int_{\lambda_+}^{\kappa_2} u_{III}(\xi)\, \xi\, d\xi \qquad \text{A-20}$$

For the plug region $\lambda_- < \xi < \lambda_+$:

$$\phi_{II} = \int_{\lambda_-}^{\lambda_+} u_{II}(\xi)\, \xi\, d\xi \qquad \text{A-21}$$

The total dimensionless flow rate is given by,

$$\phi_{tot} = \phi_I + \phi_{II} + \phi_{III} \qquad \text{A-22}$$

The mass is set to be conserved if the following condition is satisfied,

$$\left|\frac{\phi_{tot} - \phi_{pipe}}{\phi_{pipe}}\right| \leq \epsilon_2 \qquad \text{A-23}$$

Appendix B: Numerical model

The force balance on a fluid element flowing in the annular space can be written as,

$$\frac{1}{\mathrm{r}}\frac{\mathrm{d}(\mathrm{r}\tau)}{\mathrm{dr}} = -\frac{\mathrm{dp}}{\mathrm{dz}} \qquad \text{B-1}$$

Where the shear stress is given in terms of apparent viscosity (μ) as,

$$\tau = \mu\dot{\gamma} \qquad \text{B-2}$$

Equation (B-2) is substituted into Eq. (B-1), the following expression is obtained,

$$\frac{d}{dr}\left(\mu\frac{dv}{dr}\right) + \frac{\mu}{r}\frac{dv}{dr} = -\frac{dp}{dz} \qquad \text{B-3}$$

$$\left(\frac{1}{\mu}\frac{d\mu}{dr}\right)\frac{dv}{dr} + \frac{d^2v}{dr^2} + \frac{1}{r}\frac{dv}{dr} = -\frac{1}{\mu}\frac{dp}{dz} \qquad \text{B-4}$$

The Finite difference method was used to discretize this equation with central scheme at the interior points and backward and forward scheme at the boundaries. The derivative in the first term in Eq. (B-4) is discretized as written in Eq. (B-5), which makes the scheme stable [27].

$$\frac{1}{\mu}\frac{d\mu}{dr} = \frac{d\, log\mu}{dr} = \frac{\log(\mu)_{i+1} - \log(\mu)_{i-1}}{2\,\Delta r} = A \qquad \text{B-5}$$

After discretizing, Eq. (B-4) becomes,

$$A\left(\frac{v_{i+1} - v_{i-1}}{2\,\Delta r}\right) + \frac{v_{i+1} - 2\,v_i + v_{i-1}}{\Delta r^2} + \frac{1}{r_i}\frac{v_{i+1} - v_{i-1}}{2\,\Delta r} = -\frac{1}{\mu_i}\frac{dp}{dz} \qquad \text{B-6}$$

Rearranging,

$$\left[\frac{A}{2\,\Delta r} + \frac{1}{\Delta r^2} + \frac{1}{2\,r_i\,\Delta r}\right]v_{i+1} - \left[\frac{2}{\Delta r^2}\right]v_i + \left[-\frac{A}{2\,\Delta r} + \frac{1}{\Delta r^2} - \frac{1}{2\,r_i\,\Delta r}\right]v_{i-1} = -\frac{1}{\mu_i}\frac{dp}{dz} \qquad \text{B-7}$$

$$A_n\, v_{i+1} + A_p\, v_i + A_s\, v_{i-1} = b_i \qquad \text{B-8}$$

The following boundary conditions are used,

At $(r = r_p)$, $v_{(i=0)} = v_p$

At $(r = r_h)$, $v_{(i=n_g)} = 0$ (n_g is the number of grid points)

References

[1] Mitchell R. Dynamic surge/swab pressure predictions. SPE Drilling Engineering, 1988; 3(03): 325-333.

[2] Crespo F, Ahmed R, Enfis M, Saasen A, and Amani M. Surge-and-swab pressure predictions for yield-power-law drilling fluids. SPE Drilling & Completion, 2012; 27(04): 574-585.

[3] Crespo F and Ahmed R. A simplified surge and swab pressure model for yield power law fluids. Journal of Petroleum Science and Engineering, 2013; 101: 12-20.

[4] Erge O, Akin S, and Gucuyener I. Accurate modeling of surge and swab pressures of yield power law fluids in concentric annuli. in SPE/IADC Middle East Drilling Technology Conference and Exhibition, 2018: OnePetro.

[5] Burkhardt J. Wellbore pressure surges produced by pipe movement. Journal of petroleum technology, 1961; 13(06): 595-605.
[6] Schuh F. Computer makes surge-pressure calculations useful. Oil and Gas Journal, 1964; 31: 96–104.
[7] Chukwu GA. Surge and swab pressure computed for couette flow of power-law fluids. 1990; OSTI Identifier:6200808.
[8] Osorio F, and Steffe J. Evaluating Herschel-Bulkley fluids with the back extrusion (annular pumping) technique. Rheologica acta, 1991; 30(6): 549-558.
[9] Haige W and Xisheng L. Study on steady surge pressure for yield-pseudoplastic fluid in a concentric annulus. Applied Mathematics and Mechanics, 1996; 17(1): 15-23.
[10] Cannon GE. Changes in Hydrostatic Pressure Due to Withdrawing Drill Pipe from the Hole. in Drilling and Production Practice, 1934: American Petroleum Institute.
[11] Goins Jr W, Weichert J, Burba Jr J, Dawson Jr D, and Teplitz A. Down-the-hole pressure surges and their effect on loss of circulation. in Drilling and Production Practice, 1951: American Petroleum Institute.
[12] Cardwell Jr W. Pressure changes in drilling wells caused by pipe movement. in Drilling and Production Practice, 1953: American Petroleum Institute.
[13] Clark Jr E. A graphic view of pressure surges and lost circulation. in Drilling and Production Practice, 1956: American Petroleum Institute.
[14] Fontenot JE, and Clark R. An improved method for calculating swab and surge pressures and circulating pressures in a drilling well. Society of Petroleum Engineers Journal, 1974; 14(05): 451-462.
[15] Lubinski A, Hsu F, and Nolte K. Transient pressure surges due to pipe movement in an oil well. Revue de l'Institut Français du Pétrole, 1977; 32(3): 307-348.
[16] Lal M. Surge and swab modeling for dynamic pressures and safe trip velocities. in IADC/SPE Drilling Conference, 1983: Society of Petroleum Engineers.
[17] He S, Srivastav R, Tang M, and Ahmed R. A new simplified surge and swab pressure model for yield-power-law drilling fluids. Journal of Natural Gas Science and Engineering, 2016; 28: 184-192.
[18] Ferroudji H, Hadjadj A, Ofei TN, Rahman MA., Hassan I, and Haddad A. CFD method for analysis of the effect of drill pipe orbital motion speed and eccentricity on the velocity profiles and pressure drop of drilling fluid in laminar regime. Pet Coal, 2019; 61(5): 1241-1251.
[19] Ferroudji H, Hadjadj A, Rahman MA, Hassan I, Maheshwari P, and Odan MA. Study of Ostwald-de Waele fluid flow in an elliptical annulus using the slot model and the CFD approach. Journal of Dispersion Science and Technology, 202142(9): 1395-1407.
[20] Razi MM, Mazidi M, Razi FM., Aligolzadeh H, and Niazi S. Artificial neural network modeling of plastic viscosity, yield point, and apparent viscosity for water-based drilling fluids. Journal of dispersion science and technology, 2013; 34(6): 822-827.
[21] Rooki R. Estimation of pressure loss of Herschel–Bulkley drilling fluids during horizontal annulus using artificial neural network. Journal of Dispersion Science and Technology, 2015; 36(2): 161-169.
[22] Krishna S, Ridha S, and Vasant P. Prediction of Bottom-Hole Pressure Differential During Tripping Operations Using Artificial Neural Networks (ANN). in Intelligent Computing and Innovation on Data Science: Springer, 2020, pp. 379-388.
[23] Bourgoyne AT, Millheim KK, Chenevert ME, and Young FS. Applied drilling engineering. Society of Petroleum Engineers Richardson, TX, 1986.
[24] API13D, Rheology and Hydraulics of Oil-well Fluids, SIXTH ed. (API RECOMMENDED PRACTICE 13D). API Washington, DC, 2010.
[25] Beverly C, and Tanner R. Numerical analysis of three-dimensional Bingham plastic flow. Journal of non-newtonian fluid mechanics, 1992; 42(1-2): 85-115.
[26] Mendes PRS, and Dutra ES. A viscosity function for viscoplastic liquids. Annual Transactions of the Nordic Rheology Society, 2004; 12: 183-188.
[27] Chin WC. Managed pressure drilling: modeling, strategy and planning. Gulf Professional Publishing, 2012.
[28] Hussain QE, and Sharif MA Viscoplastic fluid flow in irregular eccentric annuli due to axial motion of the inner pipe. The Canadian Journal of Chemical Engineering, 1997; 75(6): 1038-1045.
[29] ANSYSFluent, ANSYS Fluent User's Guide. USA: ANSYS, Inc, 19R3.
[30] Tu J, Yeoh GH, and Liu C. Computational fluid dynamics: a practical approach. Butterworth-Heinemann, 2018.

[31] Liu Y, Wang Y, and Zhang J. New machine learning algorithm: Random forest. in International Conference on Information Computing and Applications, 2012, pp. 246-252: Springer.
[32] Pedregosa F, Varoquaux G, Gramfort A, Michel V, Thirion B, Grisel O, Blondel M, Prettenhofer P, Weiss R, Dubourg V, Vanderplas J, Passos A, Cournapeau D, Brucher M, Perrot M, and Duchesnay E. Scikit-learn: Machine learning in Python. Journal of Machine Learning Research, 2011; 12: 2825-2830.

To whom correspondence should be addressed: Dr. Zakarya Belimane, Laboratory of Petroleum Equipment's Reliability and Materials, Hydrocarbons and Chemistry Faculty, Université M'Hamed Bougara, Boumerdès, Algeria, E-mail: z.belimane@univ-boumerdes.dz